Grain boundary segregation in Dy doped ceria by TEM and laser-assisted 3D atom probe

Fang Li (李 芳)

Laboratory of Optical Information and Technology, School of Science,
Wuhan Institute of Technology, Wuhan 430074, China
**Corresponding author: lifang_wit@hotmail.com*

Received March 14, 2012; accepted July 23, 2012; posted online September 23, 2012

A combination of transmission electron microscopy (TEM) and laser-assisted three-dimensional atom probe (3DAP) is employed to study the nanostructure of Dy-doped CeO_2, which is a promising ionic conductor. Segregation of Dy atoms at grain boundaries is observed by electron energy loss spectroscopy (EELS) elemental maps. The segregation is checked and confirmed by laser-assisted 3DAP. Moreover, the enrichment of Dy and deficiency of Ce at grain boundaries are quantitatively identified by the 3DAP concentration profile. Data such as these are significant to optimize the electrical conductive property in rare-earth doped Ceria.

OCIS codes: 160.5690, 350.0350.
doi: 10.3788/COL201210.S21601.

Recently, rare-earth (RE)-doped ceria compounds with cubic fluorite structure are now under active investigation for the relatively high ionic conductivity, which can be used as an electrolytic material in "intermediate" (300–500 °C) temperature solid oxide fuel cells (SOFCs)[1−4]. Although the RE-doped ceria shows considerable promise as SOFCs, its electrical conductivity is not as high as expected. So many studies should be carried out to optimize the electrolytic property. Until now, it has been demonstrated that the grain size and grain boundary have significant influence to the electric conductivity. In Sm-doped CeO_2[5] and Y-doped CeO_2 eletrolytes[6], it was found the overall conductivity decreased due to the grain boundary resistivity increase by decreasing the grain size. Nevertheless, in Gd-doped CeO_2 electrolytes[7], it was found that the conductivity improved by decreasing grain size from 3 to 0.7 μm. More recently, Ou *et al.*[8,9] found that the overall conductivity decreases with decreasing the grain size if the RE-doped ceria has coarser grains, and increase with decreasing the grain size if the RE-doped ceria has finer grains.

Actually, when changing the grain size, the grain boundaries resistivity changes, that is the real reason why grain size influences the conductivity. So the grain boundaries resistivity has really significant influence on the overall conducting properties. In polycrystalline ceramic materials, the grain boundary resistivity has been proposed to result from different segregated elements[10] and the variation of grain boundary structure[11], but there is no directly confirmative experimental work was conducted. The detailed microstructure information about the grain boundaries remains unclear. So there is a high necessary to further explore what is the nanostructure of grain boundaries and whether there is segregation at grain boundaries in order to optimize the electrolytic properties. In this letter, we analyze the nanostructure of Dy-doped CeO_2 by a combination of TEM with electron energy loss spectroscopy (EELS) and laser-assisted three-dimensional atom probe (3DAP).

The sample of bulk ceramic Dy doped CeO_2 was prepared by a previously reported method[12]. In Brief, the nano-sized powders of $Dy_{0.2}Ce_{0.8}O_{1.9}$ were firstly prepared using ammonium carbonate co-precipitation method; and then for conventional sintering (CS), these powders were molded under a pressure of 500 kg/cm^2 and subjected to a rubber press 2 t/cm^2 in order to obtain a green body. CS temperature was 1 450 °C for 6 h. Finally, compact discs with a diameter of 10 mm and a thickness of 2 mm were prepared from the calcined powders and sintered at the temperature of 1 450 °C for 6 h.

TEM specimen was prepared by mechanical polishing and dimpling, followed by ion milling method. TEM observation was carried out using a FEI Tecnai G^2 F30 with Gatan imaging filter Tridiem. The jump ratio method was employed to obtain elemental maps using the Ce:$N_{4,5}$(110 eV), Dy:$N_{4,5}$(154 eV), and O:K (532 eV) edges. Atom probe specimen was prepared by the focused ion-beam (FIB) lift-out technique and a SEM/FIB annular milling procedure. A final sharp needle-shaped tip with a radius of curvature smaller than 100 nm was obtained. The details of the process have been reported[13,14]. The 3DAP data were obtained by a locally built straight type 3DAP instrument with CAMECA's fast delay line detector[15]. The laser source for atom probe was a femtosecond laser (343 nm, 400 fs, 2 kHz) with laser energy of 0.1 μJ/pulse and laser spot size of ∼150 μm. The atom probe analyses were carried out under the following conditions: tip temperature ∼60 K, background pressure ∼1×10^{-8} Pa, evaporation rates 0.1–0.2 ion/pulse.

Figure 1 is the bright-field TEM image of Dy doped CeO_2, which shows a polycrystalline structure with an average grain size of ∼200–400 nm. In order to check whether there is elemental segregation at grain boundaries, we carried out EELS measurement. Figure 2 shows the EELS elemental maps of Dy-doped CeO_2. Figure 2(a) is the zero loss image, showing a grain boundary tri-junctions region. Figure 2(b) is the elemental map of Ce. The presence of dark contrast along grain boundaries indicates Ce-poor. Figure 2(c) shows the elemental map of Dy. It can be seen that a bright contrast along

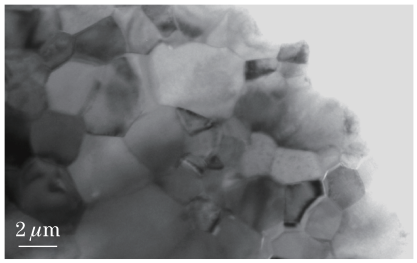

Fig. 1. Bright filed transmission electron image of Dy-CeO_2, showing a polycrystalline structure with an average grain size of ∼200–400 nm.

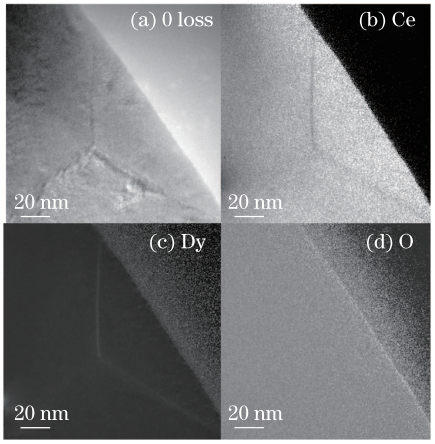

Fig. 2. EELS maps of Dy-CeO_2 for (a) zero loss image which shows a grain boundary tri-junctions region, elemental map of (b) Ce, (c) Dy, and (d) O.

the grain boundaries, which indicates Dy-rich. Figure 2(d) is elemental map of oxygen. No obvious contrast can be seen, which shows oxygen uniformly distributed inside the grain and at the grain boundary tri-junctions region. In Figs. 2(b) and (c), it should be noted that three grain boundaries appear different contrast due to the different angles between observation beam and grain boundaries' orientation. Herein, we confirmed that there was elemental segregation at the grain boundaries, and got a qualitatively result that Dy was rich and Ce was poor at the grain boundaries. In order to further confirm the segregation and get quantitative results of the elemental distributions, we performed laser-assisted 3DAP analysis.

The laser-assisted 3DAP is the only method that enables elemental mapping in three-dimensional space with atomic scale resolution. Figure 3 shows the 3D reconstructed atom maps of Dy (green), Ce (red), and oxygen (blue), with a volume of about 45×10×120 (nm). The reconstructed volumes were oriented in order to image the grain boundary tri-junctions perpendicular to the plane of view. Note that there is strong contrast along the grain boundaries, which implies a different composition or different concentration at the grain boundary. In order to determine the composition of these regions, three sampling boxes A, B, and C were used (Fig. 3). Furthermore, three composition profiles were plotted vertically across three grain boundaries, as shown in Figs. 4(a), (b), and (c), respectively. Each composition measurement was taken from a different number of atoms, and so there is no fixed uncertainty, however, the errors associated with each point are ± 2%–3%, as can be seen from the statistical fluctuation in profiles.

The composition profile taken from selected box A is shown in Fig. 4(a). It can be seen that there is a significantly higher Dy concentration and lower that Ce concentration at the grain boundary region. This result is well consistent with the EELS observation. From the concentration profile, we can further know the average concentrations of Dy and Ce in the grains are about 12 at.-% and 35 at.-%, respectively. While the maximum concentration of Dy is 24 at.-% and the minimum concentration of Ce is 19 at.-% at the grain boundary. So Dy concentration at the grain boundary is 12 at.-% higher than that in the grains, and Ce concentration at the grain boundary is 16 at.-% lower than that in the grains. In case of oxygen atoms, there is no obvious variation at the grain boundaries, and the average concentration value is about 53 at.-%.

Figure 4(b) shows the composition profile taken from selected box B. It also indicates a higher Dy concentration and lower Ce concentration along the grain boundary. The average concentrations of Dy and Ce in the grains are about 12 at.-% and 38 at.-%, respectively. While the maximum concentration of Dy is 17 at.-% and the minimum concentration of Ce is 32 at.-% at the grain boundary. So Dy concentration at the grain boundary is 5 at.-% higher than that in the grains, and Ce concentration at the grain boundary is 6 at.-% lower than that in the grains. Similarly, in case of oxygen atoms, there is no obvious variation at the grain boundaries, and the average concentration value is about 50 at.-%.

The composition profile taken from selected box C is shown in Fig. 4(c). Similarly, a higher Dy concentration and lower Ce concentration at the grain boundary region can be observed. The average concentrations of Dy and Ce in the grains are about 12 at.-% and 36 at.-%, respectively. While the maximum concentration of Dy is 21 at.-% and the minimum concentration of Ce

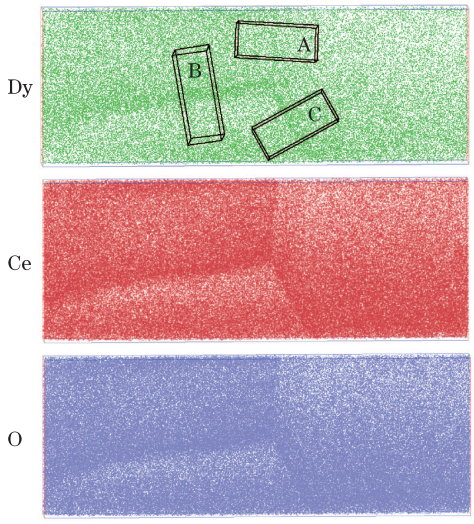

Fig. 3. 3D atom maps of Dy, Ce, and O atoms (volume of ∼45×10×120 (nm)) with schematic of sampling boxes A (volume of ∼10×8×22 (nm), B (volume of ∼9×8×25 (nm)), and C (volume of ∼10×8×22 (nm)).

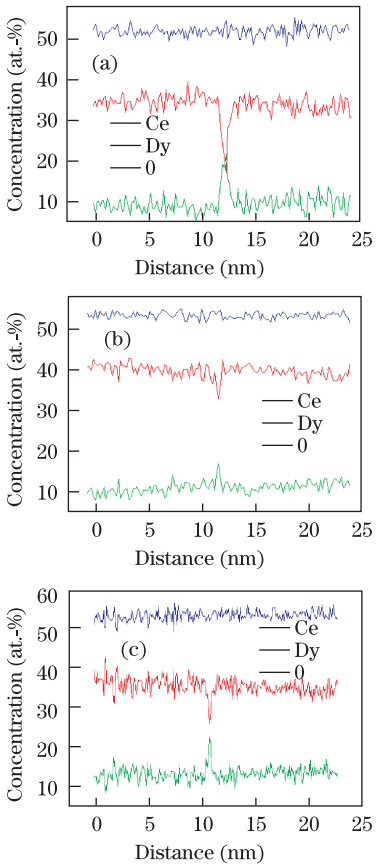

Fig. 4. Composition profiles calculated from selected box (a) A, (b) B, and (c) C.

is 25 at.-% at the grain boundary. So Dy concentration at the grain boundary is 9 at.-% higher than that in the grains, and Ce concentration at the grain boundary is 11 at.-% lower than that in the grains. In case of oxygen atoms, there is no obvious variation at the grain boundaries, and the average concentration value is about 52 at.-%.

All of the three composition profiles clearly indicate the enrichment of Dy at the grain boundaries, which are in agreement with the EELS elemental mapping. These segregation behaviors could result from many processes during high temperature annealing, i.e., recrystallization, dopant diffusion along grain boundaries and so on. The enrichment of Dy along the grain boundaries would certainly increase the barrier height, resulting in an increase of the resistivity of the grain boundaries. Detailed discussion should be carried out about the electrical characteristics of the Dy-doped CeO_2.

In conclusion, we investigate the nanostructure of Dy doped CeO_2 by a combination of TEM and laser-assisted 3DAP. It is confirmed that Dy is enriched and Ce is deficit along grain boundaries. More importantly, the dopant enrichment is quantitatively obtained by laser-assisted 3DAP technique. It is useful to help explain and optimize the electrolytic property of RE-CeO_2.

This work was supported by the National Natural Science Foundation of China under Grant No. 11204222.

References

1. B. C. H. Steele and A. Heinezl, Nature **414,** 345 (2001).
2. H. Inaba and H. Tagawa, Solid State Ionics **83,** 1 (1996).
3. G. B. Balazs and R. S. Glass, Solid State Ionics **76,** 155 (1995).
4. K. Eguchi, T. Setoguchi, Y. Inoue, and H. Arai, Solid State Ionics **52,** 165 (1992).
5. G.-B. Jung and T.-J. Huang, J. Mater. Sci. **38,** 2461 (2003).
6. C. Tian and S. Chan, Solid State Ionics **134,** 89 (2000).
7. G. Christie and F. Berkel, Solid State Ionics **83,** 17 (1996).
8. D. R. Ou, T. Mori, F. Ye, M. Takahashi, J. Zou, and J. Drennan, Acta Materialia **54,** 3737 (2006).
9. T. Mori and J. Drennan, J. Electronceram **17,** 749 (2006).
10. M. J. Verkerk, A. J. A. Winnubst, and A. J. Burggraaf, J. Mater. Sci. **17,** 3113 (1982).
11. X. Guo, Solid State Ionics **81,** 235 (1995).
12. T. Mori, R. Buchanan, D. R. Ou, F. Ye, T. Kobayashi, J. D. Kin, J. Zou, and J. Drennan, J. Solid State Electrochem **12,** 841 (2008).
13. M. Kodzuka, T. Ohkubo, K. Hono, F. Matsukura, and H. Ohno, Ultramicroscopy **109,** 644 (2009).
14. Y. M. Chen, T. Ohkubo, M. Kodzuka, K. Morita, and K. Hono, Scripta Materialia **61,** 693 (2009).
15. G. DaCosta, F. Vurpillot, A. Bostel, M. Bouet, and B. Deconihout, Rev. Sci. Instrum. **76,** 1007 (2005).